Available online at www.sciencedirect.com
ScienceDirect
Journal of the European Ceramic Society 30 (2010) 2781–2790
www.elsevier.com/locate/jeurceramsoc

# Combustion synthesis of TiC–NiAl composite by induction heating

X. Zhu, T. Zhang *, D. Marchant, V. Morris

*Faculty of Engineering, Kingston University, Roehampton Vale, Friars Avenue, London SW15 3DW, United Kingdom*

Received 21 January 2010; received in revised form 11 April 2010; accepted 3 June 2010

**Abstract**

The aim of this work was to develop a new process for the synthesis of TiC and NiAl/TiC composite in which the combustion reaction was ignited using a high frequency induction heater. High density, two-layer TiC–NiAl composites were also produced using this process. Temperature profiles during synthesis were measured with an IR thermometer and a high resolution thermal image camera was used to monitor the reaction process. Phase transformation was investigated using XRD and SEM was used to characterize the microstructure of the synthesized composites. The mechanical properties of the products were evaluated by measuring hardness. The results show that the reaction was complete and that stoichiometric products of NiAl and TiC were produced. The properties of NiAl/TiC composites were found to be functions of composition and processing parameters. The reaction mechanism was analyzed using temperature monitoring, thermodynamic analysis and microstructure investigation.


*Keywords:* Combustion synthesis; Intermetallics; Carbide; Ceramic composite

## 1. Introduction

The high wear resistance and excellent anti-oxidation performance of TiC have attracted wide research interest and, as a result, have boosted its application in the creation of bulk components and coatings.[1] Self-propagating high-temperature synthesis (SHS) is considered to be an economic method for the synthesis of ceramics and intermetallics, with the advantage of producing products of high purity owing to the inherently elevated temperature of the SHS process.[2–5] Yeh et al. have studied the effects of TiC particles on the combustion behaviour in NiAl synthesis.[6] However, the porosity of TiC fabricated via the SHS process has restricted its application. In order to overcome this problem, Gao et al. investigated the possibility of increasing the density of TiC using a NiAl/TiC composite. The results showed that the density was significantly improved and the four-point bending strength was as high as $670 \pm 80$MPa.[7]

Although positive results on utilizing SHS for the production of dense NiAl/TiC composite have been obtained in the past, the densification mechanism was not clear and no detailed information on process control was available. The reaction sequence for the powder mixture is important since two separate exothermic reactions are needed to form NiAl and TiC. To obtain a comprehensive understanding of this issue, Curfs et al. conducted a series of studies relating to the synthesis of NiAl/TiC.[8] Results from the early studies showed that TiC and NiAl were the only synthesized products and analysis of the results showed that the synthesis started with TiC and was followed by the slow formation of NiAl.[8] However, this conclusion is contrary to evidence from the same author's later research into the combustion synthesis of NiAl, which showed that NiAl was formed with the disappearance of Ni.[9] This discrepancy was investigated further by Ren et al. who found that the TiC was surrounded by solidified NiAl crystal but the sequence of the reaction could not be determined from the experimental results.[10]

Recently several new techniques such as field-active self-propagating combustion,[11] high energy laser,[12] and solar power[13] have been introduced to initiate the combustion synthesis. However, induction heating has not been directly utilized for the ignition of combustion synthesis. When compared to other ignition sources induction heating is a fast and clean process that requires less complex equipment but has special requirements concerning the properties of the raw materials. In this study, induction heating was directly used to ignite the combustion reaction of Ni, Al, Ti and C powder compacts for the synthesis of NiAl/TiC composite. The synthesis mechanism

* Corresponding author. Tel.: +44 2085478103; fax: +44 2085478103.
*E-mail address:* t.zhang@kingston.ac.uk (T. Zhang).

0955-2219/$ – see front matter © 2010 Elsevier Ltd. All rights reserved.
doi:10.1016/j.jeurceramsoc.2010.06.002

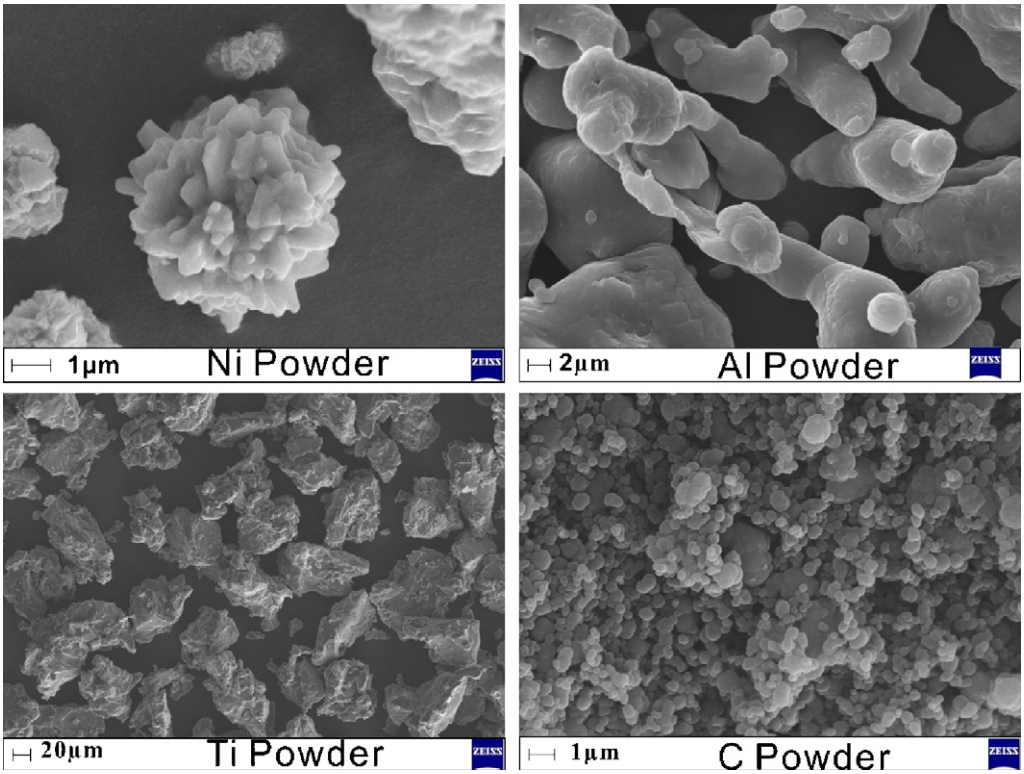


Fig. 1. Morphology of raw materials.

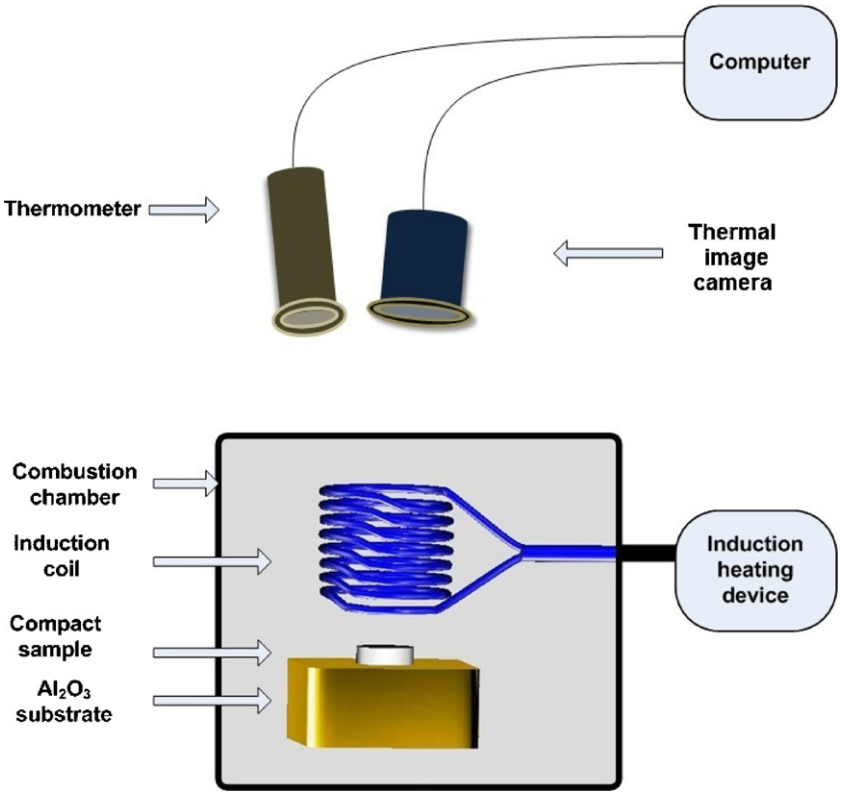


Fig. 2. Schematic diagram of experimental setting up.

Table 1
Raw materials.

| Materials | Supplier | Particle size | Purity % |
|---|---|---|---|
| Nickel powder | INCO® Carbonyl Ni Type 123 | 4.5 μm | 99.85 |
| Aluminium powder | AlPOCO® | 15 μm | 99.7 |
| Titanium powder | William Rowland | 48 μm | 98 |
| Carbon black | William Rowland | <1 μm | 99 |

of NiAl/TiC composite and two-layer NiAl/TiC will also be discussed.

## 2. Experimental details

The chemical compositions and particle sizes of the relevant raw materials are listed in Table 1 and the morphologies of all powders are shown in Fig. 1.

The experimental samples were organised into two groups: single-layer and two-layer. In the single-layer group all powders in the designated composition were fully mixed and compressed into one pellet. Ni and Al powders in the stoichiometric mole ratio 1:1 were wet mixed together with 5 wt%, 10 wt%, 15 wt% and 20 wt% of Ti/C (1:1 mole ratio) in acetone. The mixture was placed in an oven at 80 °C for 1 h to vaporize the acetone. The powder mixtures were then cold compressed in a steel die of 16 mm diameter at a pressure of 100 MPa. Each compacted pellet weighted approximately 1 g. In the two-layer group, the same powder preparation method was used for the Ni/Al and Ti/C mixtures which were then compressed separately, each layer weighing approximately 0.5 g. The Ni/Al pellet was placed under the Ti/C mixture.

A VarioCAM® high resolution thermal imaging camera was used to investigate the behaviour of the powder mixture under induction heating and to monitor the combustion propagation. A setting of 50 frames per second was used for temperature monitoring. IRBIS®3 professional software (by InfraTec) was used for the data analysis. Two infrared thermometers, Raytek® Raynger MX (temperature range 0–910 °C) and Raytek® Marathon MM (temperature range 540–3000 °C) were chosen to monitor the complete temperature profiles during synthesis. The data recording times were set at 0.1 s and 0.01 s, respectively. A schematic diagram of the experimental set-up is shown in Fig. 2. The induction heating equipment used in this study was manufactured by Cheltenham Induction Heating Limited (model EH-2.0) with maximum power of 2 kW. A helix shaped coil was selected for the test and the frequency was fixed at 387 KHz.

The crystalline structure of the raw materials and the sintered products was characterized by X-ray diffractometry (SIEMENS D500) using Cu $K_\alpha$. Samples were mounted in epoxy resin and polished for microstructure observation which was undertaken using scanning electron microscopy (SEM, Zeiss 50). The micro-hardness test was conducted at 0.01 N loading for 10 s. At least five tests were performed for each sample.

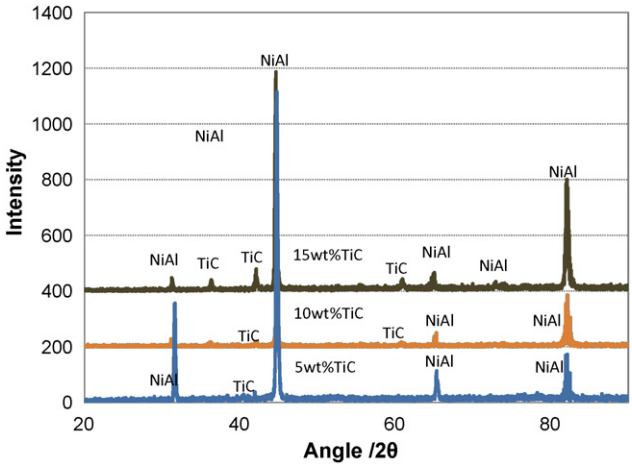


Fig. 3. The X-ray spectra of products.

## 3. Results and discussion

### 3.1. Synthesis of NiAl and TiC composites

Compacted samples with 5–20 wt% of Ti/C were heated by induction heating as described in Section 2. Intensive combustion was observed in the 5 wt%, 10 wt% and 15 wt% samples, but no combustion reaction was observed for the mixture with 20 wt% of Ti/C. To verify the reaction products, X-ray diffraction tests were carried out on both the green compacts and the heated samples. The X-ray spectra for the 5–15 wt% of Ti/C samples are shown in Fig. 3. The X-ray spectra revealed that NiAl and TiC were the only phases existing in the products with no raw materials being present in the spectra. For the sample with 20 wt% of Ti/C, the spectrum was the same as that of the raw material, indicating that no combustion reaction took place after heating. This result implies that only NiAl/TiC composites with a TiC content of less than 15 wt% can be successfully synthesized by induction heating.

### 3.2. Combustion reaction under induction heating

The full temperature profiles for the samples of Ni/Al and Ti/C mixtures are presented in Fig. 4. The average heating rates

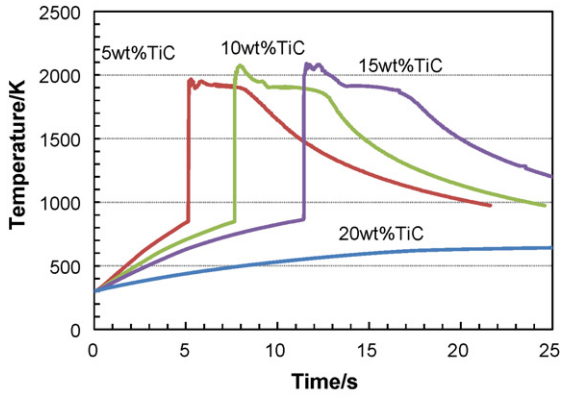


Fig. 4. Temperature profile of samples during synthesis.

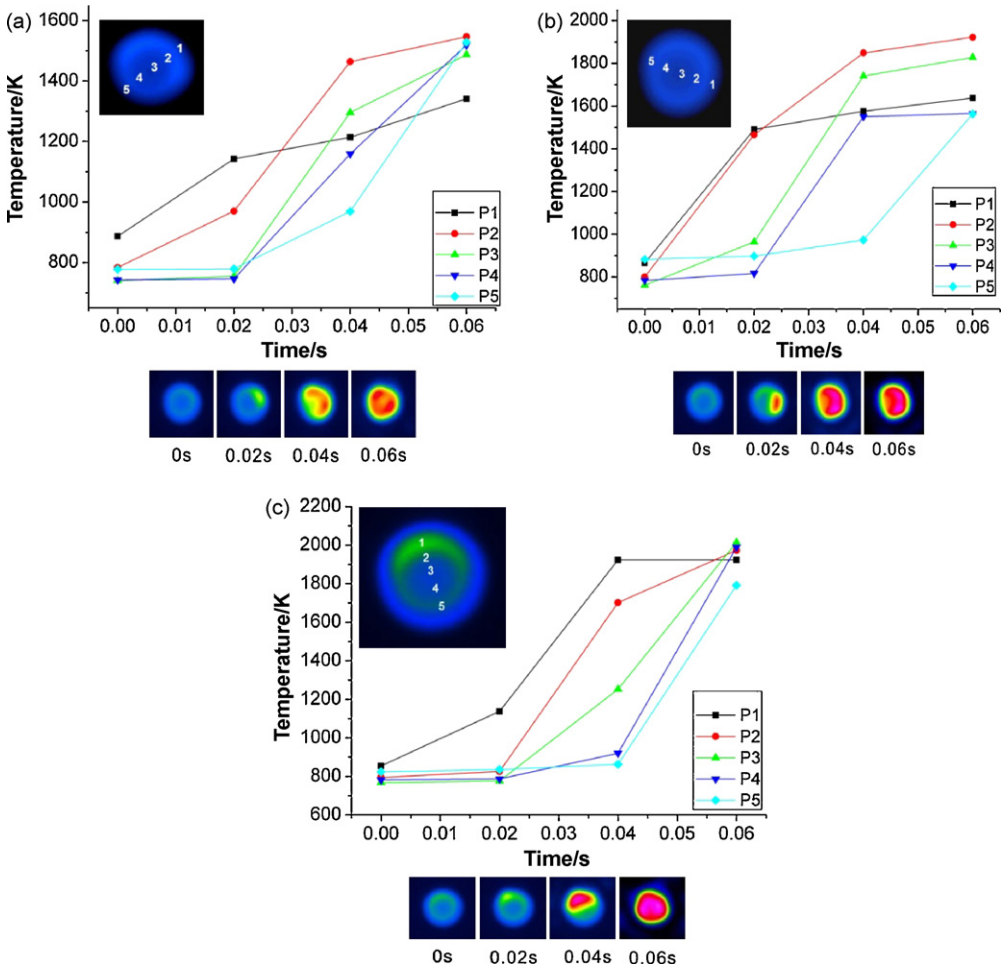


Fig. 5. Thermal images and temperature profiles during synthesis: (a) 5 wt% TiC; (b) 10 wt% TiC; (c) 15 wt% TiC.

before ignition commenced for the 5 wt%, 10 wt% and 15 wt% samples were 109.2 K/s, 72.2 K/s and 50.6 K/s respectively indicating that heating rates decrease with increased Ti/C content. For the 20 wt% sample there was no sharp increase in temperature which is consistent with the XRD test result discussed previously.

The effect of Ti/C content on the heating rate can be explained by the mechanism of induction heating and the physical properties of the materials used. The electrical efficiency under induction heating $\eta$ can be described as:

$$\eta = \frac{1}{1 + (D_1/D_2)\sqrt{\rho_1/\mu r \rho_2}} \quad (1)$$

where $D_1$ and $D_2$ are respectively the effective coil inside diameter and the diameter of the sample, $\rho_1$ and $\rho_2$ are the electrical resistivities of the coil and the sample; and $\mu_r$ is the relative magnetic permeability of the sample. Eq. (1) shows that the electrical efficiency will reduce when the relative magnetic permeability is reduced. Since Ti and C powders are non-electromagnetic materials, the addition of Ti/C will reduce the relative magnetic permeability of the compacts. As a result, an increase in the quantity of Ti/C will decrease the electrical efficiency thus resulting in a reduction of the heating rate. However, due to a lack of data on the properties of the compressed compacts, the real efficiency values cannot be quantified. Further discussion on the combustion reaction will be given in Section 3.2.

In order to monitor ignition and combustion propagation, thermal images were recorded during heating and combustion reaction. Fig. 5 shows the thermal images for the samples with 5 wt%, 10 wt% and 15 wt% Ti/C. To aid the analysis of combustion propagation, temperatures at five points in the direction of combustion propagation were also recorded and are given in Fig. 5. To provide complete coverage of the entire sample, the five points were positioned on the surface at intervals of 3 mm.

Prior to ignition (time zero in Fig. 5 and before the sharp rise illustrated in Fig. 4), the thermal images showed that there was a temperature difference in the compressed samples which reduced when the content of Ti/C was increased. When the Ti/C contents were increased from 5 wt% to 15 wt%, the temperature difference reduced from 150 K to 30 K. This difference is due to the nature of induction heating which relies on induced electrical current within the material to produce heat. When an alternating current is supplied to the coil near to the sample, a corresponding current $I_w$ is induced in the sample which does not distribute itself uniformly but concentrates at the outer ring in a phenomenon known as the skin effect. The current density reaches maximum at the outer ring of the workpiece and falls rapidly towards the centre. As a result, the outer ring was heated

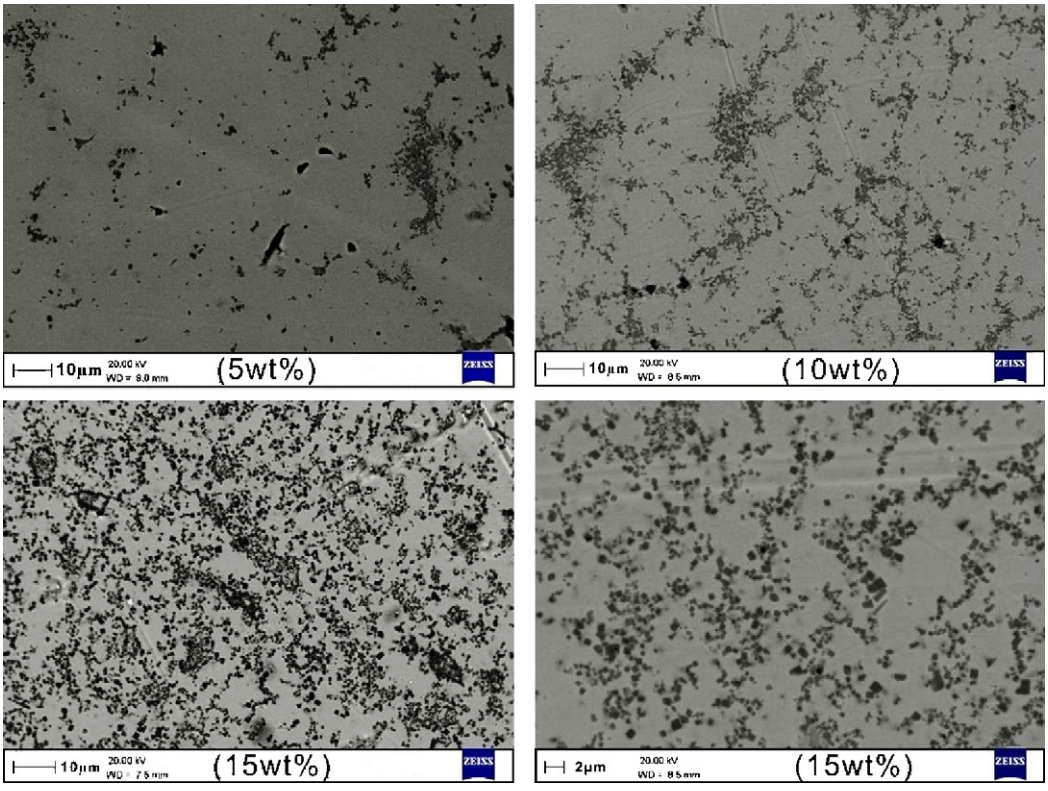


Fig. 6. Microstructure of NiAl/TiC samples: (A) NiAl rich area and (B) TiC rich area.

more quickly than the centre. The temperature distribution in the sample is also affected by heat transfer in the components. Since Ti and C are non-electromagnetic materials, their addition will reduce the relative magnetic permeability, $\mu_r$ of the compacts resulting in an increase in the skin depth (proportional to $1/\mu_r^{0.5}$) and a corresponding reduction in the heating rate at the outer ring. As shown in Fig. 4, the increase of Ti/C content reduces the heating rate of the components and hence a longer time will be required for heat to propagate within the sample. Thus, these two joint effects, non-uniform heating and heat transfer within the components, will reduce the temperature difference within the compacts during heating. The temperature difference of 20 K at the inner area (2 mm away from the outer ring) was not considered significant when compared with that of 700 K for the whole area prior to the commencement of ignition. Meanwhile, the temperature at the ignition position (outer ring) was approximately 120 K higher than that of the central area. It should be noted that the temperature distribution was not fully symmetrical about the axis of the disc because the magnetic field was not concentric owing to the shape of the coil.

For all of the reacted specimens the combustion wave propagation was completed within 0.06 s. The combustion propagation model, however, varied slightly with different Ti/C contents. For the 5 wt% and 10 wt% samples, the combustion started at the outer position and then split into two wave fronts propagating around the periphery. The 15 wt% sample also ignited at the edge but continued with one combustion front which spread into the entire sample until the propagation was completed. This behaviour occurred for two reasons: (a) there was a higher energy concentration at the outer ring for the sample with a lower Ti/C content; (b) for the 15 wt% sample, the heating time prior to ignition was longer than that of the other two samples and hence the temperature distribution was more even. This can be clearly seen in Fig. 4 for the temperature curves of the five points on the samples.

The temperature profiles shown in Fig. 5 can be used to estimate the combustion propagation velocity. Using the measured dimension of the sample, the combustion propagating velocity was estimated to be approximately 0.2–0.3 m/s. Another noticeable feature of Fig. 4 is that the maximum combustion temperature increases with increasing content of Ti/C. For the 5 wt% Ti/C sample, the maximum combustion temperature was about 1950 K, whilst that of the 10 wt% and 15 wt% samples exceeded 2100 K.

In the cooling stage after reaching peak temperature, each sample maintained a short temperature plateau at about 1920 K, which is close to the melting temperature of NiAl (1911 K). Therefore, these plateaux indicated the solidification of NiAl. The duration of the plateau increased from 3.5 s to 6 s as the Ti/C content increased from 5 wt% to 15 wt% as a result of the higher liquid content owing to the raised combustion temperature.

### 3.3. Microstructure and synthesis mechanism for TiC

The microstructure of the synthesized NiAl/TiC composites was observed using SEM, in back scatter mode, and is presented in Fig. 6. In back scatter mode, the matrix phase, NiAl, appears brighter than the TiC phase. The distribution of TiC phase was

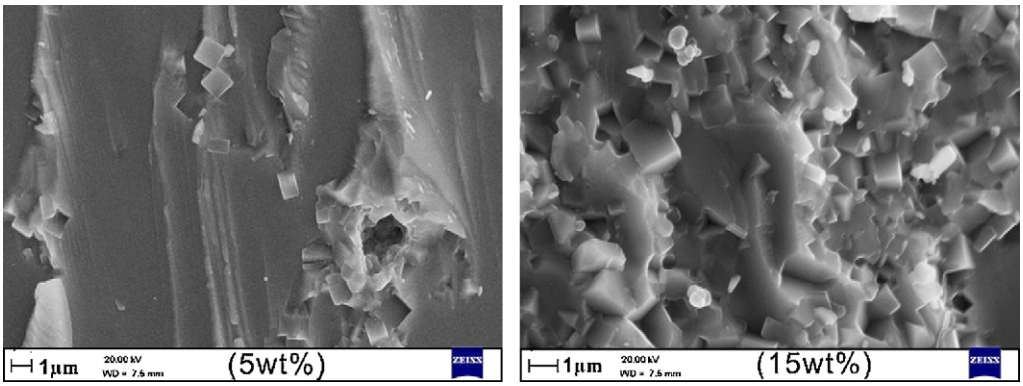


Fig. 7. Fracture surface of 5 wt% TiC and 15 wt% TiC specimen. Both were taken from TiC rich area.

heterogeneous. It was concentrated at the NiAl boundary which indicates that NiAl was synthesized before the formation of TiC. During the synthesis of TiC, the heat generated by the reaction can further melt NiAl. Therefore, some TiC particles were embedded in NiAl. Further discussion for the formation mechanism is given in Section 3.6. Fig. 6 also shows that with the increase of Ti/C content, pore sizes were reduced. The 15 wt% Ti/C sample was almost fully densified. These results can be explained by studying the thermal history during synthesis. As shown in Fig. 4, by increasing the content of Ti/C from 5 wt% to 15 wt%, the peak temperature increased from 1950 to 2100 K and the time during which the temperature remained above the melting point of NiAl (1911 K) increased from 3.5 s to 6.0 s. The consequence was to increase the liquid content, reduce the viscosity and provide a longer time for liquid flow. These joint effects contributed to the densification of the synthesized products.

By comparing the morphologies of TiC particles and the raw materials together with the temperature monitoring results (Fig. 4), the synthesis mechanism of TiC by combustion can be derived. The average particle size of TiC, as shown in Figs. 6 and 7, was less than 1 μm, which is close to the particle size of carbon powder (average 1 μm) but is much smaller than the particle size of Ti (48 μm). In addition, the fracture surfaces of the 5 wt% and 15 wt% TiC sample in Fig. 7 show that TiC particles were not only distributed at the NiAl boundary, but also embedded within the NiAl grains, which indicates that NiAl is in liquid state when TiC is formed. The temperature monitoring results (Fig. 4) show that as the Ti/C content increases the temperature rises to above the melting point of Ti (1941 K). In addition there is a decrease in the heating rate near to the melting temperature of Ti which indicates that the heat produced by the Ni/Al reaction was absorbed by the melting of Ti. At the turning point, the temperature continued to rise owing to the combustion reaction of Ti + C. Based on this analysis, the liquid synthesis mechanism should be the dominant synthesis route for TiC formation. The crystal morphology of each TiC particle was regular cubic and the size was increased slightly when the Ti/C content was increased. However, the temperature duration near to the melting temperature of Ti is very short (less than 1 s) which prevented the growth of TiC particles. As a result, the particle size of TiC formed in this process was less than 1 μm.

The fracture surfaces shown in Fig. 7 were taken from a TiC rich areas to show the fracture behaviour and the morphology of TiC particles. In the 5 wt% Ti/C sample, the dominant fracture mechanism was NiAl transgranular fracture. Because of its average sub-micron particle size, the TiC obstructed the fracture propagation. In the 15 wt% Ti/C specimen, although the NiAl transgranular fracture was the main fracture mechanism, cracks along the TiC boundary were also observed. This result suggests that, with increased TiC content, the hardness of the composites should rise, however, continued addition of TiC may result in reduced ductility. The results also show a tendency for TiC particle size increase as its content increased, which is a direct result of combustion temperature as shown in Fig. 4.

Micro-hardness testing was conducted on the samples, and the results are given in Fig. 8. There is an obvious tendency that the increase of TiC content elevated the hardness of the synthesized NiAl/TiC composite since the hardness of NiAl synthesized under the same experimental conditions was approximately 324 HV which is much lower than that of TiC (about 3000 HV). Due to the non-homogeneous distribution of TiC phase, the hardness of 5 wt% Ti/C and 10 wt% Ti/C samples fluctuated between slightly fluctuant, namely 459 ± 37 HV and 511 ± 29 HV, respectively. Compared with the value of NiAl without Ti/C addition, the hardness of 5 wt% Ti/C sample increased by approximately 50%. For the 15 wt% Ti/C sample the hardness increased to 526 ± 15 HV which is an increase of 62% on the non-Ti/C addition sample.

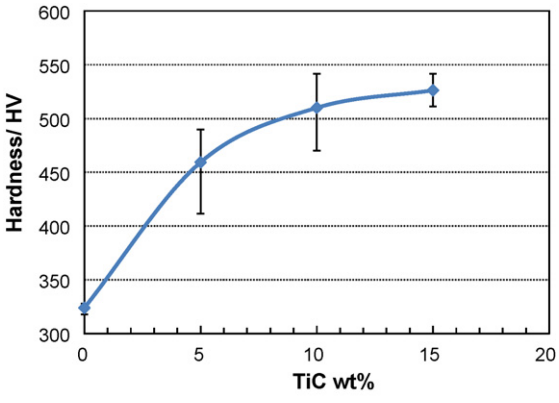


Fig. 8. Micro-hardness of NiAl/TiC composites.

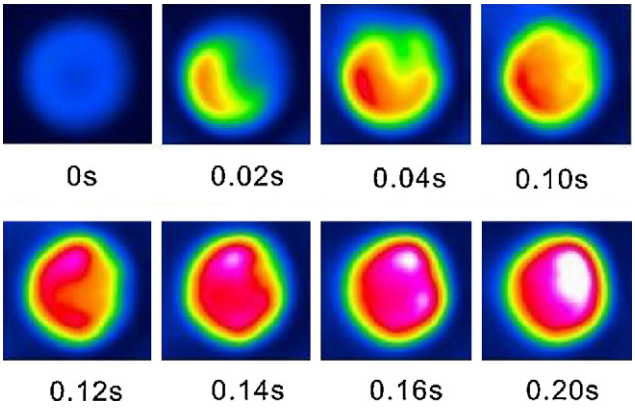


Fig. 9. Thermal images of two-layer sample during combustion reaction.

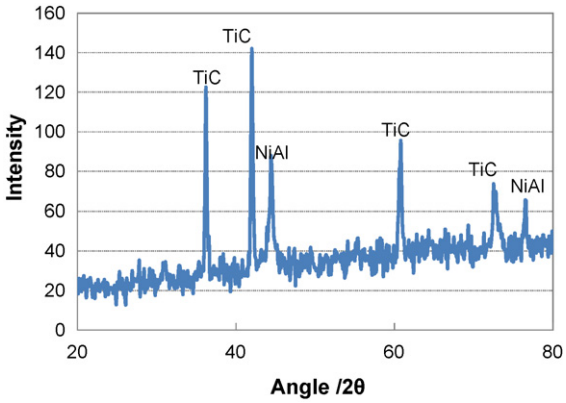


Fig. 10. XRD pattern of two-layer products.

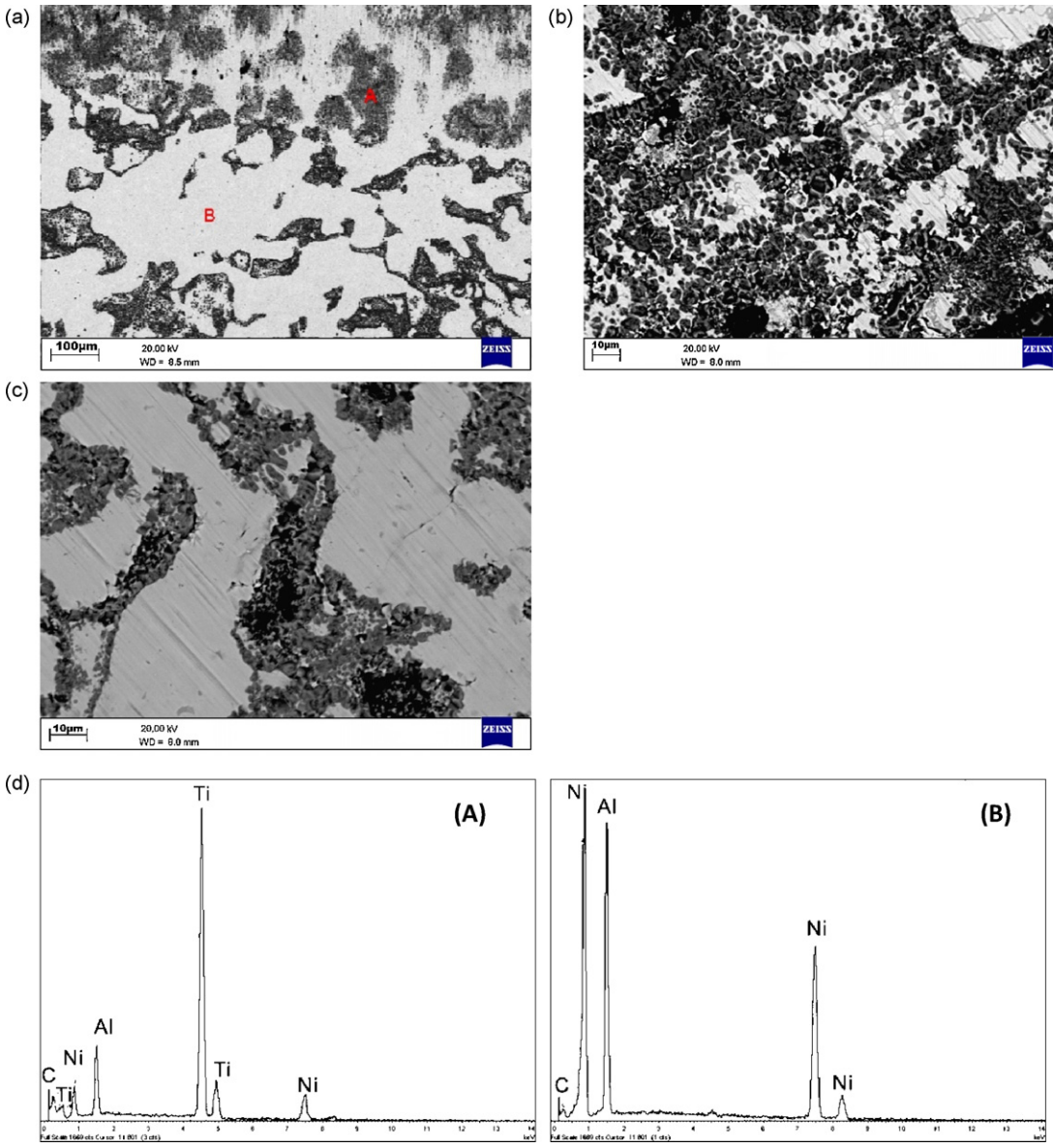


Fig. 11. Microstructure of two-layer product: (a) two-layer product; (b) TiC rich area; (c) NiAl rich area; (d) EDX at positions A and B as shown in (a).

### 3.4. Synthesis of two-layer composite

#### 3.4.1. Combustion reaction

The research work described in Section 3.1 has shown that the combustion reaction of Ti + C ignited by the reaction of Ni + Al and TiC can be synthesized to form a NiAl/TiC composite provided that the content of TiC is limited to 15 wt% with this ignition setting. To produce composites with a higher TiC content, a compressed Ti/C disc was placed on top of a compressed Ni/Al disc and then heated using the induction heating described in Section 2.

A preliminary test showed that the Ti/C mixture was insufficiently heated through induction heating indicating that, in the two-layer case, the upper layer receives heat from Ni + Al layer. Since the combustion temperature of Ti + C is extremely high (3210 K), and the reaction rate is very rapid, it was difficult to accurately record the combustion temperature. As a result, temperature monitoring using the thermal image technique was only conducted at the heating stage for the two-layer synthesis. The results are given in Fig. 9. Unlike the mixed pellet reaction in Fig. 5, there were two combustion propagations in the two-layer product synthesis. Starting from 0 s the first combustion propagated from left to right and completed after 0.10 s, this was followed by the onset of the second propagation at 0.12 s. The second combustion propagated in the same direction as the first and completed at 0.16 s. The thermal images also indicated that the second combustion temperature was much higher than the first one. Since the thermal image was taken on the surface of Ti/C compact, the temperature on the Ni/Al could not be recorded.

The test showed that combustion reaction was successfully performed as expected. The combustion reaction of Ti + C was ignited by the combustion of Ni + Al. The synthesized product was cut through the centre and the cross-section was examined using XRD. Fig. 10 shows the XRD pattern of the two-layer product. It shows that TiC and NiAl were successfully synthesized and no raw materials remained in the final product.

#### 3.4.2. Microstructure

Fig. 11a shows the back scatter microstructure of the two-layer product. The upper layer comprised the Ti + C pellet and the base layer the Ni + Al mixture. The interface between the two layers was dense and no pores were observed. Both layers contain bright and dark areas, suggesting that there was a mixing between the two layers during the combustion reactions. Fig. 11b and c shows the microstructure of the upper and base layers, respectively. EDX analysis (Fig. 11d) shows the brighter area was Ni/Al and dark area contained Ti/C and Ni/Al, strengthening the conclusion. The mixing between NiAl and TiC was clearly due to the melting of Al, Ni, NiAl and Ti since the combustion temperature of Ni/Al is higher than the melting temperature of Al and Ni and combustion temperature of the second reaction (Ti/C) was much higher than the melting temperature of NiAl and Ti.

### 3.5. Thermal dynamics analysis for the NiAl/TiC system

The temperature monitoring results given in Fig. 4 show the reaction temperature for the NiAl/TiC system is a function of Ti/C content. This function can be determined via thermo dynamic calculation. In the experiment, the X-ray spectra results showed the synthesis was complete and all the raw materials were fully consumed. The products contained only two compounds NiAl and TiC. Therefore, the reactions can be simplified as (data reference[14,15]):

$$\mathrm{Ni} + \mathrm{Al} \rightarrow \mathrm{NiAl} + 118.5\,\mathrm{kJ}$$

$$\mathrm{Ti} + \mathrm{C} \rightarrow \mathrm{TiC} + 183.8\,\mathrm{kJ}$$

In addition, the reaction velocity was fast (<0.2 s), which implies that the reactions can be treated as adiabatic. From energy conservation, the enthalpy change for the heating and combustion reaction can be described as:

$$\sum_i n_i H(R_i) = \sum_j m_j H(P_j) \tag{2}$$

where $R_i$, $P_j$ refer to the appropriate reactants and products, respectively, and $n_i$, $m_j$ are the stoichiometric coefficients of the reactants and products. In this study, prior to combustion, the whole compacted sample was heated by induction heating to different temperatures, thus the preheating energy should be added into the calculation. The preheating temperature (temperature before ignition) varies with composition and is not uniform due to the nature of induction heating. To simplify the calculation, a uniform temperature was used since the calculation is only to demonstrate the effect of Ti/C contents. To sum up, three assumptions were applied to estimate the maximum combustion temperature $T_{ad}$, as listed below:

- All of the raw materials were consumed and the products contain NiAl and TiC only;
- the combustion reaction was adiabatic;
- all pellets were preheated uniformly prior to ignition.

The same method as described by Munir et al.[5] was used to calculate $T_{ad}$ using the data given in Table 2. At 1911 K, the solid to liquid phase transition for NiAl will start and the phase transition enthalpy is 57.6 kJ/mole. Based on the literature,[16] in the temperature range 1000–3290 K, the heat enthalpy of TiC can be described as:

$$H_{\mathrm{TiC}}(\mathrm{solid}) = 43.27T + \frac{4.54446T^2}{2} + \frac{2.0214T^3}{3} - \frac{0.0203272T^4}{4} - \frac{1.701881}{T} + 184.0960 \tag{3}$$

where $T$ = temperature (K)/1000.

The combustion temperature can be calculated using Eq. (2). Fig. 12 shows the calculated $T_{ad}$ as a function of Ti/C content and preheating conditions. Since there is no reliable data for the thermal properties of liquid NiAl above 1911 K, Eq. (3) for the solid state was used to continue the calculation (Table 2).

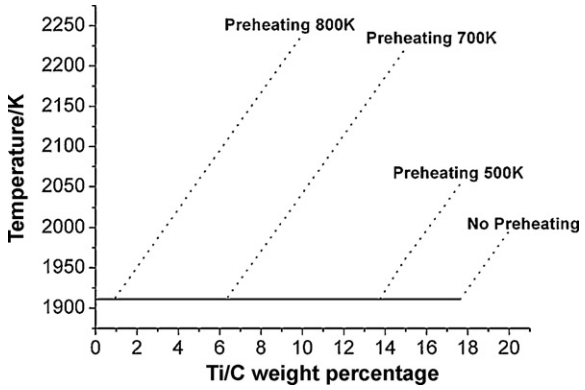


Fig. 12. Calculated combustion temperature as a function of Ti/C content and preheating temperature.

The curves above 1911 K are presented in the figure using a dashed line. The results show that the preheating has a significant effect on $T_{ad}$, when the addition of Ti/C is below 18 wt%. Without preheating, the combustion temperature of all the mixtures remained at 1911 K until the Ti/C content was increased to approximately 18 wt% since below this weight fraction NiAl will not fully melt. With preheating to 500 K, the minimum requirement to fully melt NiAl is reduced to 13 wt% Ti/C. Above this weight fraction $T_{ad}$ will increase linearly with Ti/C content. If the preheating temperature was increased to 700 K, the minimum requirement for Ti/C to fully melt NiAl was further reduced to 6.5 wt%, which, in turn, could be further reduced to 0.9 wt% when preheated to 800 K. The test results in Fig. 4 show all pellets were heated to above 700 K prior to ignition, therefore the reaction product NiAl should be fully melted in the samples with 10 wt% and 15 wt% Ti/C and the combustion temperature should be higher than 1911 K. This calculated result correlates well to the measured temperatures given in Fig. 4.

### 3.6. Reaction mechanism of the combustion synthesis

The intrinsically fast reaction velocity and elevated temperature of the combustion synthesis limited the investigation on the reaction mechanism. Previously, time-resolved XRD techniques and "Quench" methods have been used to analyze the synthesis process. In the literature,[8] the author utilized a time-resolved XRD to investigate the combustion reaction for the Ni/Al/Ti/C system. The XRD pattern showed that the disappearance of elements started from Al, as it has the lowest melting point, followed by Ni, Ti and finally C. On the other hand, for the synthesized product the author claimed the TiC appeared simultaneously with the melting of Ti whereas the NiAl emerged in a later stage.

For the combustion synthesis of TiC, Khina et al.[17] developed a diffusion control model (a "solid–solid–liquid" mechanism), which involves reaction kinetics and thermodynamics. The model was validated by structural analysis. However, the authors concluded that the model was not applicable for the synthesis of TiC. Instead they proposed a "solid–liquid" mechanism, which suggests that the formation of TiC starts at the dissolution of carbon into liquid titanium and is followed by the precipitation of TiC grains. This deduction is in good agreement with the results presented in the literature,[8] TiC occurs when Ti is melted.

The time-resolved XRD tests in the literature[8] presented the evidence that TiC appeared at 1.4 s while NiAl emerged at 4.2 s, thus the author concluded NiAl formation was slower than that of TiC. This conclusion is questionable because it ignored the limitation of the XRD technique that it can only detect crystalline phases. The later appearance of NiAl in XRD pattern may be owing to a solidification period after combustion. As shown in Fig. 12, the combustion temperature will exceed the melting point of NiAl when Ti/C content is over 18 wt% even without preheating. In the literature[8] the raw materials were mixed in mole ratio 1:1:1:1, equal to 41.14 wt% of Ti/C. With this amount of Ti/C the reaction temperature was certainly higher than the melting point of NiAl, regardless of the missing details of ignition system in the literature.[8] The fabricated NiAl would be fully melted and the liquid NiAl phase could not be detected by XRD till the sample's temperature cooled down to its crystallization point. Hence the later appearance of NiAl in XRD tests is not sufficient to determine the reaction sequence.

In the experimental work for the two-layer NiAl/TiC composite, two propagations were detected by the thermal images as shown in Fig. 9. As previously stated, the Ti/C layer cannot be adequately heated via induction heating so it may be concluded that the first combustion is the synthesis reaction of NiAl. The combustion temperature after the second reaction was above 2300 K, which corresponds to the synthesis of TiC. Owing to the melting of NiAl and heat loss to the environment through conduction and radiation, the temperature detected was much lower than the theoretical temperature for the adiabatic synthesis of TiC. The microstructure in Fig. 11 suggests that the product synthesized was a mutual infiltration of NiAl and TiC. The interface of the two layers was dense and no pores were observed.

Table 2
Thermal properties of Al and Ni element (data reference[14]).

| Element | Phase | Temperature of transition (K) | Heat of transition (kcal/g mole) | *a* (cal/g mole) | *b* (cal/g mole) | *c* (cal/g mole) | *d* (cal/g mole) |
|---|---|---|---|---|---|---|---|
| Al | Solid | 931.7 | 2.57 | 4.94 | 2.96 | – | – |
| | Liquid | 2600 | 67.9 | 7.0 | – | – | – |
| NI | Solid α | 626 | 0.092 | 4.06 | 7.04 | – | – |
| | Solid β | 1728 | 4.21 | 6 | 1.8 | – | – |
| Ti | Solid α | 1155 | 0.950 | 5.25 | 2.52 | – | – |
| C | Solid | – | – | 4.10 | 1.02 | – | −2.10 |

This is because NiAl had melted at the boundary and spread into the Ti/C layer during the formation of TiC. As shown in Fig. 12, the heat generated by the formation of TiC should be able to provide sufficient heat to fully melt the synthesized NiAl. Hence the reaction sequence may be stated as: Ni/Al mixture was heated by induction heating and ignited; the released energy melted Ti and then initialized the combustion reaction of Ti/C, which is accompanied by the melting and flow of NiAl. The melting of Ti leads to the formation of fine TiC grains whereas the melting and flow of NiAl results in fully densified TiC/NiAl composites.

## 4. Conclusion

A new ignition process for the synthesis of TiC was developed in this study. The combustion reaction was ignited using a high frequency induction heater. High density, multi-layer TiC–NiAl composites were produced using this method. The results show:

(a) With addition of Ti/C 1:1 weight percentage 5 wt%, 10 wt% and 15 wt%, the reaction products were pure NiAl and TiC.
(b) To ignite the combustion reaction by induction heating for the Ni/Al + Ti/C system, there is a limit for the content of Ti/C above which the ignition will not start. The peak temperature during reaction increases with increasing Ti/C content.
(c) NiAl can be fully melted in the NiAl/TiC composites during combustion reaction. As a result, fully densified NiAl/TiC composites can be produced. The hardness of synthesized NiAl can be significantly improved by the addition of Ti/C.
(d) The microstructure analysis, temperature measurements and comparison with the literature suggest the formation of TiC follows a liquid synthesis mechanism. The TiC was formed after the melting of Ti, so that nanostructured TiC can be produced.
(e) The reaction sequence for the Ni/Al/Ti/C system can be stated as: Ni/Al mixture was heated by induction heating which ignited its combustion; the energy released melted Ti and initialized the combustion reaction of Ti/C which lead to the formation of TiC and it is accompanied by the melting of NiAl.

## References


1. David RL. *CRC handbook of chemistry and physics*. CRC Press; 2007–2008.
2. Moreno B, Chinarro E, Jurado JR. Combustion synthesis of the cermet $LaCrO_3$–Ru. *J Eur Ceram Soc* 2008;**28**:2563–6.
3. Kexin C, Haibo J, Heping Z, Ferreira JMF. Combustion synthesis of AlN–SiC solid solution particles. *J Eur Ceram Soc* 2000;**20**:2601–6.
4. Marin-Ayral RM, Pascal C, Martinez F, Tedenac JC. Simultaneous synthesis and densification of titanium nitride by high pressure combustion synthesis. *J Eur Ceram Soc* 2000;**20**:2679–84.
5. Munir ZA, Anselmi-Tamburini U. Self-propagating exothermic reactions: the synthesis of high-temperature materials by combustion. *Mater Sci Res* 1989;**3**:279–365.
6. Yeh CL, Su SH, Chang HY. Effects of TiC addition on combustion synthesis of NiAl in SHS mode. *J Alloys Compd* 2005;**398**:85–93.
7. Gao MX, Pan Y, Oliveira FJ, Baptista JL, Vieira JM. Interpenetrating microstructure and fracture mechanism of NiAl/TiC composites by pressureless melt infiltration. *Mater Lett* 2004;**58**:1761–5.
8. Curfs C, Cano IG, Vaughan GBM, Turrillas X, Kvick A, Rodriguez MA. TiC–NiAl composites obtained by SHS: a time-resolved XRD study. *J Eur Ceram Soc* 2002;**22**:1039–44.
9. Curfs C, Tun-As X, Vaughan GBM, Terr AE, Kvick A, Rodriguez MA. Al–Ni intermetallics obtained by SHS; a time-resolved X-ray diffraction study. *Intermetallics* 2007;**15**:1163–71.
10. Ren KG, Chen KX, Zhou HP, Ning XS, Jin HB. Combustion synthesis of NiAl/TiC multiphase composites and their related microstructure. *Rare Met Mater Eng* 2007;**36**:848–51.
11. Xue H, Munir ZA. Synthesis of AlN—SiC composites and solid solutions by field-activated self-propagating combustion. *J Eur Ceram Soc* 1997;**17**:1787–92.
12. Hunt EM, Plantier KB, Pantoya ML. Nano-scale reactants in the self-propagating high-temperature synthesis of nickel aluminide. *Acta Mater* 2004;**52**:3183–91.
13. Sierra C, Vazquez A. NiAl coatings on carbon steel by self-propagating high-temperature synthesis assisted with concentrated solar energy: mass influence on adherence and porosity. *Sol Energy Mater Sol Cells* 2005;**86**:33–42.
14. Weast. *CRC handbook of chemistry and physics*. 68th ed. CRC Press; 1987–1988.
15. Colin J, Smithells EAB. *Metals reference book*. Butterworths London & Boston; 1976.
16. Chase Jr MW. *NIST-JANAF themochemical tables: J. Phys. Chem. Ref. Data, Monograph 9*; 1998.
17. Khina BB, Formanek B, Solpan I. Limits of applicability of the "diffusion-controlled product growth" kinetic approach to modeling SHS. *Phys B: Condens Matter* 2005;**355**:14–31.